



PCCP

Transition-metal single atoms in nitrogen-doped graphene as efficient active centers for water splitting: A theoretical study

Journal:	<i>Physical Chemistry Chemical Physics</i>
Manuscript ID	CP-ART-10-2018-006755.R1
Article Type:	Paper
Date Submitted by the Author:	12-Dec-2018
Complete List of Authors:	Zhou, Yanan; Sichuan University, School of Chemical Engineering; E O Lawrence Berkeley National Laboratory, Materials Science Division Gao, Guoping; Lawrence Berkeley National Laboratory, Berkeley, Materials Science Division Li, Yan; Xi'an Jiaotong University, School of Materials Science and Engineering Chu, Wei; Sichuan University, Chengdu 610065, School of Chemical Engineering Wang, Lin-Wang; Lawrence Berkeley National Laboratory, Materials Science Division

SCHOLARONE™
Manuscripts



Transition-metal single atoms in nitrogen-doped graphene as efficient active centers for water splitting: A theoretical study

Yanan Zhou,^{‡ab} Guoping Gao,^{‡b} Yan Li,^c Wei Chu,^{*a} and Lin-Wang Wang^{*b}

Received 00th January 20xx,
Accepted 00th January 20xx

DOI: 10.1039/x0xx00000x

www.rsc.org/

Highly active single-atom catalysts (SACs) have recently been intensively studied for their potential for hydrogen evolution reaction (HER) and oxygen evolution reaction (OER). Due to the existence of many such SACs systems, a general understanding of the trend and designing principle is necessary to discover the optimal SACs system. In this work, by using density functional theory (DFT), we investigated a series of late single transitional metals (TM=Fe, Co, Ni, Cu, and Pd) anchored on various N doped graphene (xN-TM, x=1~4) as electrocatalysts for both HER and OER. Solvent effects were taken into account by implicit continuum model. Our results reveal that the catalytic activity of SACs is determined by the local coordination number of N and TM in catalysts. Among the considered catalysts, the low-coordinated Co site, *i.e.* triple-coordinated Co, exhibits high catalytic activity toward HER with the calculated hydrogen adsorption free energy of -0.01 eV, while high-coordinated Co center, *i.e.* quadruple-coordinated Co is a promising candidate for OER with a low computed overpotential of -0.39 V, which are comparable to those of noble metal catalysts, indicating both superior HER and OER performance of N-Co co-doped graphene. The results shed light on the potential application of TM and N co-doped graphene as efficient single-atom bifunctional catalysts for water splitting, thereby offering as the promising candidate for hydrogen/oxygen production.

1. Introduction

Owing to the global energy crisis and the environmental problem caused by carbon dioxide emission in fossil fuel consumption, numerous efforts have been devoted to searching for sustainable alternative energy from renewable resources.¹⁻³ Hydrogen appears to be a promising clean energy carrier,^{4, 5} which can be generated by electrocatalytic or photocatalytic water splitting. The water-splitting reaction, which is a reverse process of fuel cell

reactions, involves two half-reactions: the cathodic hydrogen evolution reaction and the anodic oxygen evolution reaction, both of which are important for the overall feasibility of a water splitting system.^{6, 7}

Although the Pt-based materials^{8, 9} and Ru- or Ir-based compounds^{10, 11} are the state-of-the-art electrocatalysts for the HER and OER, respectively, their widespread applications are limited by their high cost and scarcity. Consequently, numerous research attempts have been devoted to developing active and stable nonprecious metal alternative electrocatalysts for HER and OER, such as non-precious metal oxides,^{12, 13} carbides,¹⁴ borides,¹⁵ nitrides,¹⁶ sulfides,^{17, 18} and phosphides¹⁹⁻²¹. Supported SACs have recently become a new research frontier and attracted considerable attention^{22, 23} because the atomic dispersion of isolated metal atoms on support surfaces can maximize the efficiency of metals and the SACs often possess excellent catalytic activity. More importantly, due to the limited atomic configurations, it is relatively easy for us to understand the nature of the active sites on SACs and identify intrinsic reaction mechanism on catalysts. In a way, the SACs combines

^a School of Chemical Engineering, Sichuan University, Chengdu, 610065, Sichuan, China

^b Materials Science Division, Lawrence Berkeley National Laboratory, Berkeley, 94720, California, United States

^c State Key Laboratory for Mechanical Behavior of Materials, Xi'an Jiaotong University, Xi'an, 710049, Shaanxi, China

*E-mail address: chuwei1965@scu.edu.cn (Wei Chu); lwwang@lbl.gov (Lin-Wang Wang)

†Electronic Supplementary Information (ESI) available: [details of any supplementary information available should be included here]. See DOI: 10.1039/x0xx00000x

‡ Both authors contributed equally.

the feature of the molecule-based homogeneous catalyst with the electric conductivity of the heterogeneous surface catalyst. However, despite of the intensive interest, the current study of SACs used for HER and OER were generally investigated separately one at a time, hence it is difficult to achieve the understanding of the trend and designing principle. It is also helpful to search for systems with bifunctional electrocatalytically properties for both hydrogen and oxygen generations to achieve sustainable overall water splitting.²⁴⁻²⁶

Graphene is a widely used substrate for electrochemical reactions that has unique physical properties, such as a large specific surface area, good stability as well as superior electrical conductivity, making it suitable as catalyst precursor and support for advanced electrocatalysts.^{27, 28} Metal dopants such as Fe or Co,^{12, 29} or non-metallic dopants such as nitrogen and boron³⁰⁻³² play an important role in the formation of functionalized catalysts for graphene. Transition-metal and nitrogen co-doped carbon-based materials have been proven to be efficient electrocatalysts for water splitting reactions.^{12, 33, 34} The metal center coordinated with nitrogen atoms were recognized as the active site for HER and OER.^{35, 36} What's more, experimental results^{19, 33, 37} confirmed that the metal-centered and nitrogen-coordinated matrix (M-N, M= cost-effective transition metal, such as Fe, Co or Ni) can have demonstrated remarkable electrocatalytic activities. The so-called M-N-based SACs have been considered as a promising substitute for the precious metal electrocatalysts.³⁸⁻⁴⁰ Recently, Guan *et. al.*⁴¹ found that mononuclear manganese embedded in N-doped graphene matrix shows high performance for HER and OER, and they ascribed the high activity to the coordination of N to manganese. Zeng *et. al.*⁴² also reported experimentally that Fe embedded into N-doped graphene possesses high performance for OER due to the dispersed highly catalytically active sites. Even though the synergistic effect between transition metal and nitrogen has been proposed to analyze the improved electrocatalytic activities,^{35, 43} it remains unclear for the exact optimal atomic coordination number of the late transition metal-nitrogen based active sites as well as the reaction mechanism and their trends for these structures.

In this work, in order to understand how coordination number of the xN-TM (x=1~4, refers to the late TM atom bonds to number of N atom) affect the electrochemical performance and to provide design principles for the bifunctional electrocatalysts for the energy conversion, we have screened a series of late transition metal atoms anchored on different N-doped graphene, to investigate their electrocatalytic activity toward both HER and OER. Five late TM atoms (TM=Fe, Co, Ni, Cu, and Pd) are considered, anchored on four different N coordinates. The

electronic properties are analyzed to reveal the mechanism of HER and OER in those catalysts. We found that the low-coordinated Co site (3N-Co) is a potential candidate for HER with the calculated hydrogen adsorption free energy of -0.01 eV, and high-coordinated Co center (4N-Co) exhibits high catalytic activity toward OER with a low computed overpotential of -0.39 V, suggesting N-Co co-doped graphene can be used as bifunctional catalyst for HER and OER.

2. Computational methods

2.1 Computational details

All the calculations were performed by the Vienna ab initio Simulation Package (VASP)^{44, 45} code using density functional theory method. Nuclei–electron interactions were described by the projector augmented wave (PAW) pseudo-potentials.⁴⁶ The generalized gradient approximation (GGA)⁴⁷ with the PerdewBurke-Ernzerhof (PBE)⁴⁸ functional was employed to describe the electron exchange-correlation interaction. The semi-empirical dispersion-corrected DFT-D2 scheme proposed by Grimme⁴⁹ was used to describe the van der Waals interaction. The spin polarization was considered throughout all the calculations. The plane wave basis set with a cutoff energy of 500 eV was used in all the computations to describe all atoms' valence electrons. The convergence tolerance for energy and force during geometrical optimization was set to 10⁻⁵ eV and 10⁻² eV/Å, respectively. A vacuum space of 20 Å was set for all the considered structures, including armchair and zigzag edges, to avoid the interactions between periodical images. To assess the stability of the SAC against metal atom aggregation, the difference between the binding energy of the metal atom (E_b) on N-doped graphene and bulk cohesive energy (E_{coh}) was calculated as a descriptor for this purpose.

$$E_b = E_{\text{substrate+atom}} - E_{\text{substrate}} - E_{\text{free-atom}} \quad (1)$$

$$E_{\text{coh}} = E_{\text{bulk}}/n - E_{\text{free-atom}} \quad (2)$$

Where, E_{substrate+atom}, E_{substrate}, and E_{free-atom} denote the total energies of free atom binds with different N doped graphene substrate, N doped graphene substrate, and the free atom, respectively. *n* is the number of atoms in the bulk. When |E_b| > |E_{coh}|, it is expected that single metal atom embedded into the substrate is energetically more favorable than the metal aggregation.⁴⁰ Given the presence of a water solvent, it can affect the energetics of different electrochemical systems,^{50, 51} the polarizable implicit solvent models were calculated with VASPsol.^{52, 53}

For HER and OER reaction intermediate state (H*, HO*, O* and HOO*) on the above xN-TM

electrocatalysts, we have tested several different initial configurations for each system, followed by atomic relaxations. The reported results refer to the most stable configurations. The adsorption energy (E_{ads}) is calculated as following equation (3):

$$\Delta E_{\text{ads}} = E_{\text{substrate + adsorbent}} - E_{\text{substrate}} - E_{\text{adsorbent}} \quad (3)$$

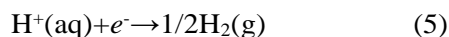
Here, $E_{\text{substrate + adsorbent}}$, $E_{\text{substrate}}$ and $E_{\text{adsorbent}}$ refer to the ground-state energies of substrate-adsorbent composites, the substrate and the adsorbent. A negative value corresponds to an exothermic process. The more negative value of ΔE_{ads} means the stronger binding between intermediate and catalyst. We have also calculated the Bader charge and charge density difference as well as d band center to further analyze the binding mechanism between the catalyst and intermediates. The charge transfer can be qualitatively visualized using the charge density difference defined as follows (4):

$$\Delta\rho = \rho_{\text{total}} - \rho_{\text{catalyst}} - \rho_{\text{adsorbent}} \quad (4)$$

Where ρ_{total} , ρ_{catalyst} and $\rho_{\text{adsorbent}}$ are the total charge densities of the adsorption system, the catalyst and the adsorbent, respectively.

2.2 Hydrogen evolution reaction

Under standard conditions, the overall HER can be described by the following equation (5):



The overall HER mechanism can be understood by a three-state diagram including an initial state $\text{H}^+(\text{aq}) + e^-$, an intermediate state with adsorbed H^* and the final product $1/2\text{H}_2(\text{g})$. At the standard electrode voltage, the total energy of $\text{H}^+(\text{aq}) + e^-$ is equal to that of $1/2\text{H}_2(\text{g})$.²⁶ That helps to define $\mu(\text{H}^+, \text{aq})$ and $V(\text{SHE})$, the proton chemical energy in the water (at $\text{pH}=0$), and the standard hydrogen electron (SHE) voltages. $\mu(\text{H}^+, \text{aq}, \text{pH}=0) + eV(\text{SHE}) = 1/2G(\text{H}_2, \text{g})$, here $G(\text{H}_2, \text{g})$ is the gas phase Gibbs free energy of H_2 , which can be calculated DFT. The HER reaction barrier (overpotential for the electron) is determined by the intermediate state energy of one H adsorbed on the catalyst. More specifically, the reaction is: $\text{Catalyst} + \text{H}^+(\text{aq}) + e^- \rightarrow \text{Catalyst}/\text{H}^*$. The extra voltages ΔV (beyond $V(\text{SHE})$) required to make this reaction happen will be the overpotential. Since $\mu(\text{H}^+, \text{aq}) = 1/2G(\text{H}_2, \text{g}) - eV(\text{SHE})$, we thus have⁵⁴: $e\Delta V(\text{SHE}) = G(\text{Catalyst}/\text{H}^*) - G(\text{Catalyst}) - 1/2G(\text{H}_2, \text{g})$. In the current study, we have ignored possible additional transition barriers between the intermediate states; instead we just use the intermediate state energies to define the catalytic barrier. In actual calculation, the above equation can also be written as⁵⁵:

$$e\Delta V = \Delta E_{\text{H}^*} + \Delta E_{\text{ZPE}} - T\Delta S_{\text{H}^*} \quad (6)$$

Where $\Delta E_{\text{H}^*} = E(\text{Catalyst}/\text{H}^*) - E(\text{Catalyst}) - 1/2E(\text{H}_2)$, ΔE_{H^*} is the hydrogen adsorption energy, ΔE_{ZPE} is the difference in zero-point energy between the adsorbed hydrogen and gas-phase hydrogen, and ΔS_{H^*} is the entropy difference between the adsorbed state and the gas phase. T is the temperature at 298K. The ($e\Delta V$) can be written as ΔG_{H^*} . Both ΔE_{ZPE} and ΔS_{H^*} can be calculated from vibrational frequencies of the system. ΔE_{ZPE} ⁵⁶ can be calculated by $\Delta E_{\text{ZPE}} = E_{\text{ZPE}}(\text{H}^*) - 1/2E_{\text{ZPE}}(\text{H}_2)$, obtained from the calculation of vibrational frequencies for the adsorbed hydrogen. In fact, the ZPE and the entropy of the adsorbed adsorbents on different catalysts are found to have close values (listed in Table S1 and 2†).

Note, following Nørskov's assumption,⁵⁴ the overpotential of HER is η^{HER} , that is $|\Delta G_{\text{H}^*}|/e$, since for negative ΔG_{H^*} , what limits the reaction is the second step when catalyst/ H^* takes another H^+ to become H_2 . The potential needed for the second step is $-\eta^{\text{HER}}$ of the first step. Thus, the overall overpotential will be η^{HER} . Thus, too weak or too strong intermediate state binding will not be good for the HER performance. This leads to the typical volcano plot. We have used the $|\Delta G_{\text{H}^*}|$ to calculate volcano curve for the theoretical exchange current i_0 to describe the HER kinetics at $U=0$ for $\text{pH}=0$ as equation (7):

$$i_0 = -ek_0 \frac{1}{1 + \exp(|\Delta G_{\text{H}^*}|/k_b T)} \quad (7)$$

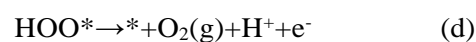
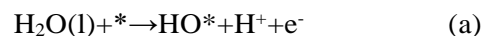
Where, k_0 is the reaction rate constant at zero overpotential, k_b is the Boltzmann constant, T is the temperature. For illustrative purpose, we have set k_0 to 1.

2.3 Oxygen evolution reaction

In the acidic environment, OER proceeds via a four-stage pathway. The overall OER can be defined as follows (8):



OER processes have the following four electron reaction paths in equations (a) - (d), as reported⁵⁷⁻⁵⁹:



Where * stands for catalyst and active sites adsorption on the catalyst, (l) and (g) refer to the liquid and gas

phase, respectively, and O*, HO* and HOO* are referred to corresponding adsorbed intermediates. The Gibbs free energy (ΔG) gains of these elementary steps when the electrode potential is at SHE level can be written as:

$$\Delta G_a = G(\text{HO}^*) + 1/2G(\text{H}_2, \text{g}) - G(\text{H}_2\text{O}, \text{l}) - G(^*) \quad (8a)$$

$$\Delta G_b = G(\text{O}^*) + 1/2G(\text{H}_2, \text{g}) - G(\text{HO}^*) \quad (8b)$$

$$\Delta G_c = G(\text{HOO}^*) + 1/2G(\text{H}_2, \text{g}) - G(\text{O}^*) - G(\text{H}_2\text{O}, \text{l}) \quad (8c)$$

$$\Delta G_d = \{4.92\text{eV} + 2G(\text{H}_2\text{O}, \text{l}) - 2G(\text{H}_2, \text{g})\} + 1/2G(\text{H}_2, \text{g}) + G(^*) - G(\text{HOO}^*) \quad (8d)$$

In deriving the above ΔG , we have used $\mu(\text{H}^+, \text{aq}, \text{pH}=0) + eV(\text{SHE}) = 1/2G(\text{H}_2, \text{g})$. For equation (d), we have also used⁶⁰: $G(\text{O}_2, \text{g}) + 4G(\text{H}_2, \text{g}) - 2G(\text{H}_2\text{O}, \text{l}) = 4.92\text{ eV}$, so we don't need to calculate the gas phase O₂ free energy since there are some possible large DFT errors for that calculation. The $G(\text{H}_2\text{O}, \text{l})$ is the liquid phase water Gibbs free energy, which is difficult to be calculated directly. It is customary to calculate the liquid phase Gibbs free energy from its vapor phase counterpart at their equilibrium pressure when they have the same Gibbs free energies. Then, $G(\text{H}_2\text{O}, \text{l}) = E_{\text{H}_2\text{O}} + \text{ZPE}_{\text{H}_2\text{O}} - \text{TS}_{\text{H}_2\text{O}}$. Here, $E_{\text{H}_2\text{O}}$ is the DFT calculated single water molecule energy in vacuum; $\text{ZPE}_{\text{H}_2\text{O}}$ is the zero point energy; $\text{TS}_{\text{H}_2\text{O}}$ is the entropy term of the gas phase (in equilibrium with the liquid phase), it includes the phonon entropy as well as gas phase translation and rotation entropy. We take the value of 0.67 eV for this $\text{TS}_{\text{H}_2\text{O}}$.⁶¹ The same for $G(\text{H}_2, \text{g}) = E_{\text{H}_2} + \text{ZPE}_{\text{H}_2} - \text{TS}_{\text{H}_2}$, here the gas phase refers to the standard one atmosphere gas phase. The TS_{H_2} are calculated with the value of 0.41 eV in Ref.⁶¹ Similarly, E_{H_2} is the DFT energy of H₂ molecule in

vacuum, and the ZPE_{H_2} is the zero energy of the phonon vibration. The same is true to the other few adsorbed species X (X=HO*, O* and HOO*), where $G(\text{X}^*) = E_{\text{X}^*} + \text{ZPE}_{\text{X}^*} - \text{TS}_{\text{X}^*}$. Here E_{X^*} is the DFT energy of the X* system under the polarization solvent model, to take into account their interaction with water. ZPE_{X^*} is the ZPE of X*. Here we only include the phonon degree of freedom in X*, while keeping the catalyst * fixed. Similarly, TS_{X^*} is the entropy term calculated with the phonon models from the adsorbed molecule. Finally, $G(^*) = E(^*)$ is the DFT calculated catalyst energy under the solvent model. Note, in all the above calculations, in the evaluation of G, we have ignored the thermal energy term due to the phonon degree of freedom. That energy can be calculated from the phonon model, just like the TS term, but it is rather small, thus has been ignored. More detailed formalism and the values for different terms are given in the supporting information.

Note, in the above four steps (a~d), each reaction is equilibrated or become possible when the electrode potential V is equal or lower than $V(\text{SHE}) - \Delta G$. Since $\Delta G_a + \Delta G_b + \Delta G_c + \Delta G_d = 4.92\text{eV}$, the best scenario corresponds to the case when they are all the same, and equals to 1.23 eV, that's the ideal catalyst. Then all the reaction will happen when V equals to the ideal $\{V(\text{SHE}) - 1.23\}$ potential. If these four ΔG are different, the overpotential η of OER (η^{OER}) is defined as the lowest potential V among the four steps, referenced by the ideal $\{V(\text{SHE}) - 1.23\}$ level. In other words, it can be defined as:

$$\eta^{\text{OER}} = \frac{\max\{\Delta G_a, \Delta G_b, \Delta G_c, \Delta G_d\}}{e} - 1.23 \quad (9)$$

The above calculations are done at pH=0. If pH is not zero, the potential V to equilibrate the reactions will all be shifted by $-k_b T \ln 10 \times \text{pH}$, where k_b is the Boltzmann constant. Additionally, we define that $\Delta G_a = \Delta G_{\text{HO}^*}$, $\Delta G_{\text{O}^*} = \Delta G_b + \Delta G_{\text{HO}^*}$, $\Delta G_{\text{HOO}^*} = \Delta G_a + \Delta G_b + \Delta G_c$, $\Delta G_d = 4.92 - \Delta G_{\text{HOO}^*}$. Thus, equation (9) can be rewritten as (10):

$$\eta^{\text{OER}} = \frac{\max\{\Delta G_{\text{HO}^*}, \Delta G_{\text{O}^*} - \Delta G_{\text{HO}^*}, \Delta G_{\text{HOO}^*} - \Delta G_{\text{O}^*}, 4.92 - \Delta G_{\text{HOO}^*}\}}{e} - 1.23 \quad (10)$$

3. Results and discussion

3.1 Atomic structures and electronic properties

To gain insight into the HER and OER catalytic mechanism on the different coordination configuration of N doped graphene with anchored TM, six categories of models for graphene with N dopant at different sites were selected from previous experimental and theoretical studies,⁶²⁻⁶⁴ as shown in

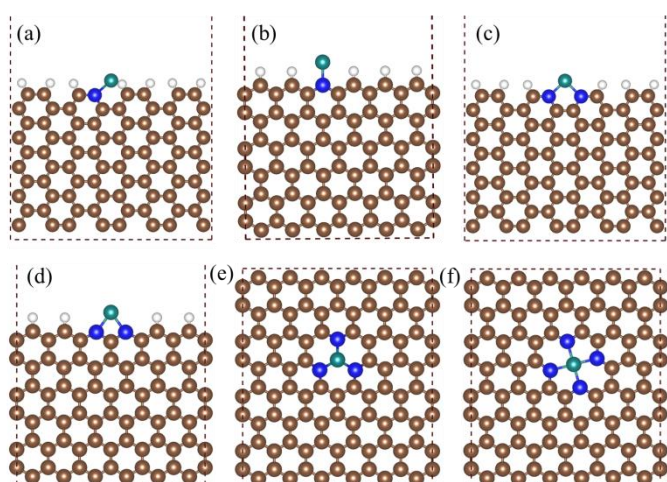


Fig. 1 Optimized graphene configurations with N dopant considered in this work: (a) 1N-AC, (b) 1N-ZZ, (c) 2N-AC, (d) 2N-ZZ, (e) 3N, and (f) 4N. The H, C, and N atoms are shown in white, brown, and blue colors, respectively.

Fig. 1. They are chosen to provide different N-coordination environment for the transition metal. They include 1N-AC (created by replacing an edge carbon atom of armchair graphene with a nitrogen atom), 1N-ZZ (created by removing an edge carbon atom of zigzag graphene with a nitrogen atom), 2N-AC (created by substituting two carbon atoms of armchair graphene with two nitrogen atoms), 2N-ZZ (created by replacing two carbon atoms of zigzag graphene with two nitrogen atoms), 3N (created by removing one C atom, and replacing the three uncoordinated carbon atoms with the nitrogen atoms), 4N (created by deleting a C-C bond and substituting the four nearest C atoms with nitrogen atoms). On top of these six different N coordination defects, one TM atom (Fe, Co, Ni, Cu, and Pd) was placed on these defect sites. The N-TM coordination number varies from 1 to 4. The single- and double-coordinated metal atom sites were built on the 1N-AC, 1N-ZZ, 2N-AC, and 2N-ZZ edges (denoted as 1N-AC-TM, 1N-ZZ-TM, 2N-AC-TM, and 2N-ZZ-TM, respectively). The triple-coordinated metal sites were developed by embedding TM atoms into the 3N defective graphene (refers to 3N-TM). TM atoms doped on the 4N formed the quadruple-ordinated metal (denotes as 4N-TM). We exhibit the optimized configurations of xN-Co ($x=1\sim4$) in Fig. S1† as one example. The binding energies of TM atoms with different coordinated active sites and their corresponding bulk cohesive energies are displayed in Fig. 2, and the detailed optimized structure parameters are listed in Table S3 and 4†.

We see that the binding strength increases with the N coordination number. While it is stable for 3N and 4N sites, for most TM, it is unstable for the lower coordination number sites. We can conclude that the

following eight xN-TM systems 3N-Fe, 3N-Co, 3N-Ni, 4N-Fe, 4N-Co, 4N-Ni, 4N-Cu, and 4N-Pd can enhance the dispersion of TM atoms significantly as their binding energies exceed their corresponding cohesive energies. Thus, the aggregation of their metal atoms can be avoided.⁶⁵ However, other systems are thermodynamic unstable due to their lower binding energies than their cohesive energies, resulting in metal clustering, which is a major problem in maintaining the stability of these systems. To further understand the binding interaction for the optimized xN-TM catalysts and their potential for HER and OER catalyst, taking the stable 3N-Co and 4N-Co systems as example, we have investigated their partial density of states (PDOS) and charge density difference after doping TM atoms. As displayed in Fig. S2a and b†, the peaks near the Fermi level indicate that both 3N-Co and 4N-Co exhibit metallic properties, which suggests good electric conductivity for the HER and OER. Additionally, the presence of p states of N atom and d states of Co around the Fermi energy indicate strong hybridization between N and Co atoms, indicating strong binding between the N and TM atoms. The strong interaction can also be inferred from the charges transfer between TM atoms and substrates as shown by Bader charge. The Bader charges analysis in Table S4† show that the charge transfer from TM atoms to substrates generally increases with the increase of coordination number, agreeing with the binding energy trend. We can also see the charge transfer trend on the charge density difference (Fig. S2c and d†), which is consistent with the results of Bader charge analysis.

3.2 HER catalytic activity

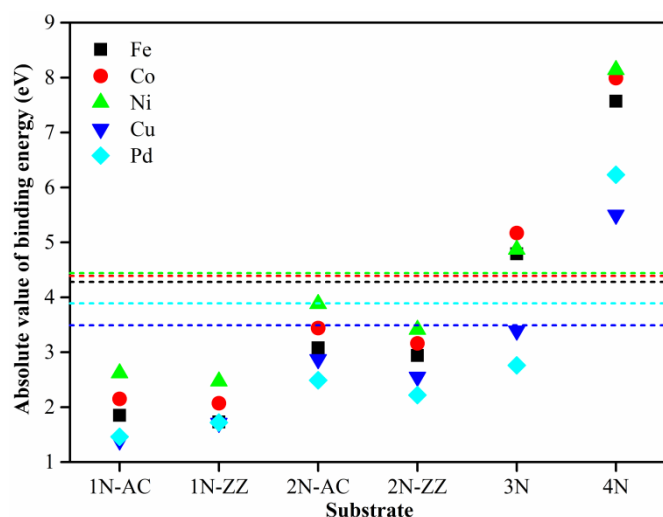


Fig. 2 The screening of promising single atom catalysts with high geometric stability. The black, red, green, blue, and cyan lines are corresponding to the cohesive energies of Fe, Co, Ni, Cu, and Pd crystals, respectively.

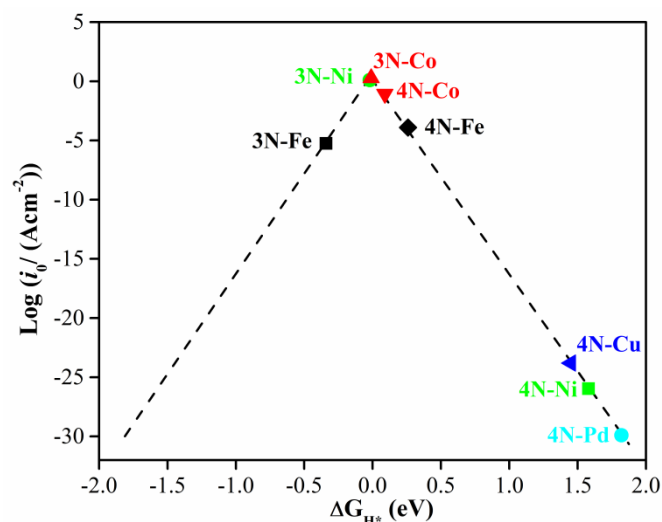


Fig. 3 The HER volcano curve of exchange current (i_0) as the function of the Gibbs free energy of hydrogen adsorption (ΔG_{H^*}) on stable 3N-TM and 4N-TM catalysts.

The Gibbs free energy for the hydrogen adsorption on the catalyst (ΔG_{H^*}) is a key descriptor for the HER activity of the catalyst.⁵⁴ For the ideal catalyst, the Gibbs free energy value for the hydrogen adsorption on the catalyst should be close to 0 eV, that is, $\Delta G_{H^*} \rightarrow 0$. As we defined, a catalyst with a positive ΔG_{H^*} value means it is not kinetically favored for hydrogen adsorbed on the catalyst. While a catalyst with a negative ΔG_{H^*} value indicates it is difficult to release the adsorbed hydrogen, thus restraining the HER activity. The calculated adsorption free energy of hydrogen atoms on xN-TM active sites are presented in Fig. S3a and b†. To compare the HER performance on stable xN-TM catalysts, a volcano curve is plotted using i_0 as a function of the ΔG_{H^*} (Fig. 3). We can quantitatively evaluate the HER performance by the position of the i_0 and ΔG_{H^*} values with respect to the volcano peak. The positive and negative values of ΔG_{H^*} are located around the right and left legs of the volcano, respectively. Furthermore, the closer the position of ΔG_{H^*} values to the volcano peak, the better HER performance of the catalyst.⁵⁴ As shown in Fig. 3, for the lower coordination 3N-Fe system, the interaction between the adsorbed H and 3N-Fe is too strong, with a negative ΔG_{H^*} value of -0.34 eV (Fig. S3a†), which indicates that the release of adsorbed hydrogen on 3N-Fe is restrained, resulting in the inhibition of HER activity. The relative large negative

ΔG_{H^*} is located at the left leg with a very low exchange current. For 3N-Co and 3N-Ni catalysts, their ΔG_{H^*} values are larger than that of the 3N-Fe catalyst, with ΔG_{H^*} values of -0.01 eV, and -0.02 eV, respectively, which are close to 0 eV. Thus, they are located around the peak of the volcano curve with the maximum exchange current. As the values of ΔG_{H^*} furtherly increase for higher coordination catalysts (4N-Co, 4N-Fe, 4N-Cu, 4N-Ni, and 4N-Pd), the exchange current i_0 decrease. Their ΔG_{H^*} values are all positive (Fig. S3b†), indicating that it is difficult for hydrogen to adsorb on these catalysts, that is, hydrogen adsorption is the rate determining step on these catalysts. Based on the above results, we can conclude that increasing the coordination number of N-TM could weak their interaction with hydrogen. To gain more insights for the HER performance for different xN-TM catalysts, the PDOS of the d band center (ϵ_d) of the different coordinated TM atoms were calculated as shown in Fig. 4. As reported, the d band center can be used to describe the interaction strength between adsorbates and catalysts.⁶⁶⁻⁶⁸ Therefore, the relationship between ϵ_d of different coordinated TM atoms and the adsorption free energies of reaction species for the HER are considered. It can be concluded that, for the high HER performance exhibited in 3N-TM catalysts, the ϵ_d shifts to lower energy with respect to the Fermi level when the

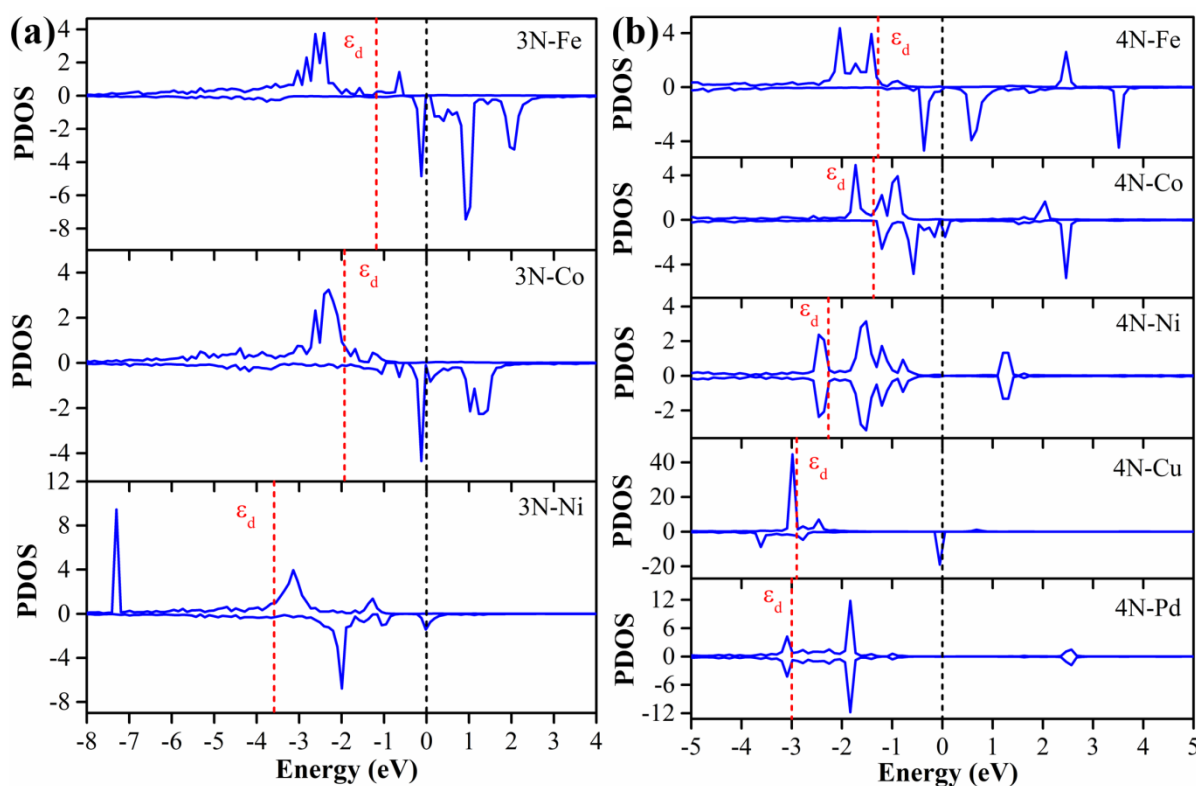


Fig. 4 Calculated PDOS of the d band of the TM in (a) 3N-TM, (TM = Fe, Co, and Ni); (b) 4N-TM, (TM = Fe, Co, Ni, Cu, and Pd). The Fermi level is set at the zero of energy and the d band center (ϵ_d) is marked by the red dash line.

atomic number of TM atoms (From Fe to Ni) increases, implying that the binding strength of H^* decrease accordingly,⁶⁹ this trend is consistent with our calculated results displayed in Table S5†. The negative correlation between ΔG_{H^*} and ϵ_d indicates that the HER performance can be well described by the trend of ϵ_d on xN-TM catalysts. Therefore, we can tune the catalytic activity to achieve the optimal HER activity by changing the coordination number of xN-TM and the d-orbital occupation of TM atoms. Overall, triple-coordinated Co atom (3N-Co) shows the highest catalytic activity performance for the HER with nearly zero value of ΔG_{H^*} (-0.01 eV). In general, 3N-TM sites exhibit a better HER performance, while, for 4N-TM systems with higher coordinated N-TM sites demonstrate poor HER performance due to their too

weak interaction with H^* , which is consistent with the theoretical results on the TM doped graphene.²⁶

3.3 OER catalytic activity

By investigating the adsorption sites on the xN-TM systems, we find that the adsorbents (HO^* , O^* and HOO^*) prefer to be adsorbed on the top of the positive charged TM atom. The adsorption free energies of adsorbents on the stable systems are summarized in Table S5†. Fig. 5 shows the Gibbs free energy differences for the OER intermediate steps occurring for the stable coordinated number catalysts. For an ideal catalyst (Fig. 5a), the energy barriers for all the steps (between two adjacent intermediate states) are all 1.23 eV. As a result, the OER can occur at its thermodynamic limit and the overpotential is zero. In

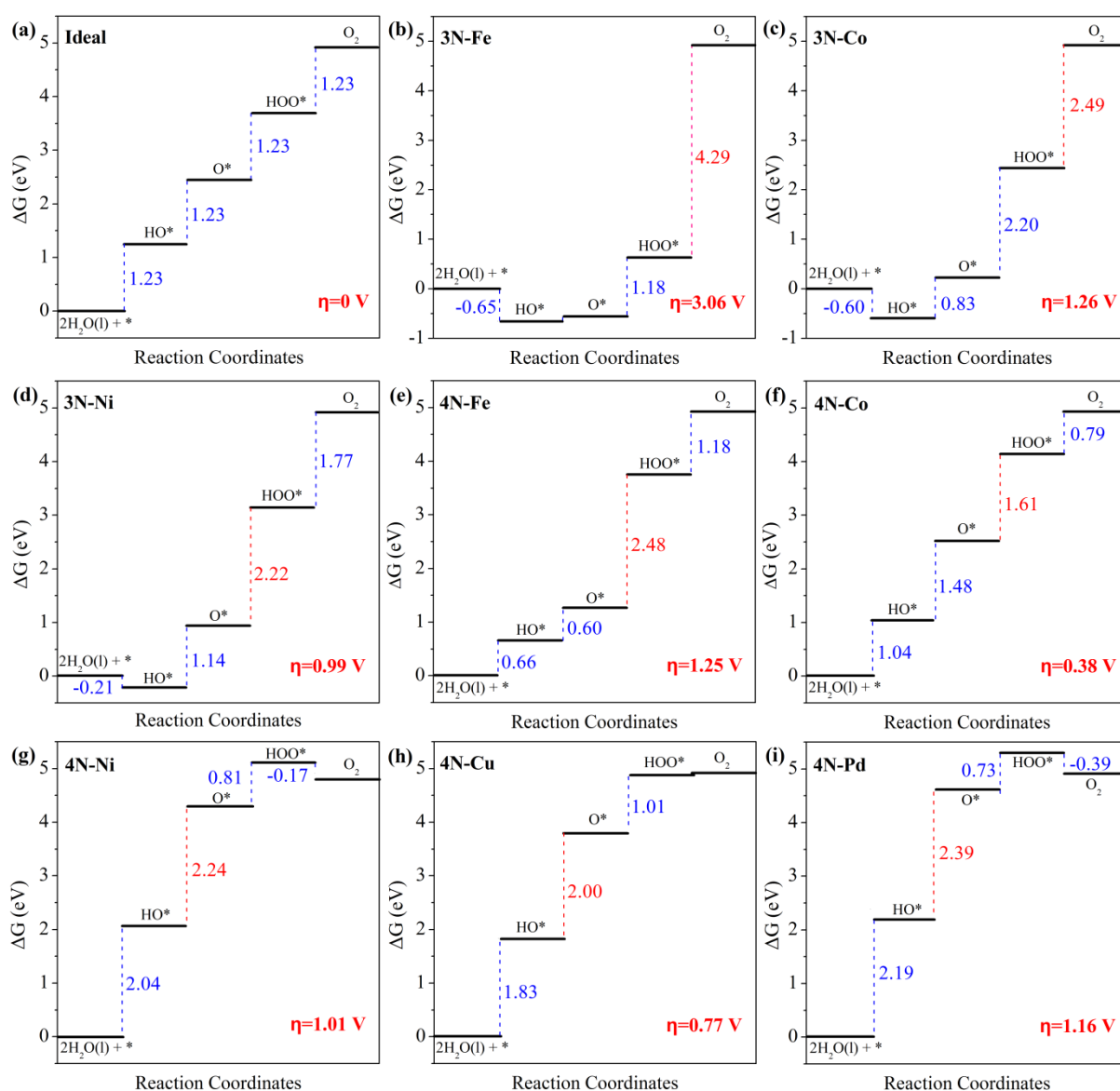


Fig. 5 The free energy diagram for OER on xN-TM at the $U = 0V$. The red line is the rate-determining step for OER. The step (Gibbs free energy difference between two intermediate states) equals to $\Delta G_{a,b,c,d}$ of equation 8a~8d.

reality, the energy steps are not equally distanced, and the overpotential η^{OER} is determined by the largest energy distance between two adjacent steps, which is labeled by the red color. It is found that the overpotential η for OER roughly decreases with the increase of the coordination number, and the ΔG_{OH^*} values are all negative when the coordination number is 3. Analyzing the triple coordinated number (3N-TM, TM=Fe, Co, and Ni) systems (Fig. 5b~d), we can find that the fourth step (release of HOO^* to O_2) of 3N-Fe and 3N-Co systems are the rate-determining steps with high energy barriers of 4.29 and 2.49 eV, respectively. The strong binding interaction of HO^* on 3N-Fe and 3N-Co catalysts with large negative ΔG_{HO^*} values lead to large positive values of ΔG_{c} and ΔG_{d} . While, for the 3N-Ni system, the interaction between HO^* and 3N-Ni is weaker than that of 3N-Fe and 3N-Co systems, resulting in a very lower positive value of ΔG_{c} . Thus, the third step ($\text{O}^* \rightarrow \text{HOO}^*$) of 3N-Ni system is the rate-limiting step with an energy barrier of 2.22 eV. In the case of 4N-TM systems (Fig. 5e~i), for the 4N-Ni and 4N-Cu, the second step ($\text{HO}^* \rightarrow \text{O}^*$) is the rate-determining step with the energy barrier of 2.24 and 2.00 eV, respectively. For the 4N-Fe and 4N-Co systems, the third step ($\text{O}^* \rightarrow \text{HOO}^*$) is the rate-determining step with an energy barrier of 2.48 and 1.61 eV, respectively. While, for the 4N-Pd systems, the first step (from $*$ to HO^*) is the rate-determining step with an energy barrier of 2.39 eV. Compared with the 3N-TM systems, we can conclude that increase the coordination number could weak the interaction between HO^* and 4N-TM catalysts. The best catalytic performance for the OER activity is identified to be quadruple coordinated Co (4N-Co) with the maximum barrier of only 1.61 eV. The corresponding optimized configurations are shown in Fig. S4†. This implies that the overpotential for the OER occurring on the 4N-Co

catalyst is only 0.38 V, which is comparable to that of the Ru-based catalysts⁷⁰ and $\gamma(\text{Ni}, \text{Fe}) \text{OOH}$.⁷¹ Furthermore, the above results also show that the OER activities are linearly related to the coordination number, that is, overpotential η for OER roughly decreases with the increase of the N-TM coordination number.

To understand the better OER performance of 4N-TM systems compared with that of 3N-TM catalysts, the adsorption free energies relationship between HO^* and HOO^* on 4N-TM systems were analyzed. We find that there is a linear relationship $\Delta G_{\text{HOO}^*} = 0.92\Delta G_{\text{HO}^*} + 3.15$ between the ΔG_{HOO^*} and ΔG_{HO^*} , with a constant of approximate 3.15 eV (Fig. 6). The slope of unity in the correlated adsorption free energies of HO^* and HOO^* suggests that both species form a single bond between O atom and the catalysts, the constant intercept indicates that both species normally prefer the same type of adsorption site.⁷² This is the so called scaling law, and is also observed on many other systems, including nitrogen-doped graphene with and without transition metal decorations.^{58, 73, 74} We know that the different OER performance originates from the different adsorption energies of HO^* , O^* , and HOO^* on xN-TM catalysts. As shown in Fig. 4, there is also a clear shift of ϵ_{d} to low-energy level with the increase of the atomic number of TMs on 3N-TM and 4N-TM catalysts, respectively, indicating that the binding strength of HO^* , O^* , and HOO^* decrease accordingly. The trend agrees well with our results shown in Table S5†. The negative correlation between ΔG and ϵ_{d} indicates that the OER performance can be well described by the trend of ϵ_{d} on xN-TM catalysts. Thus, by changing the coordination number of xN-TM and the d-orbital occupation of TM atoms, it is possible to tune the catalytic activity to achieve the optimal OER performance at N-doped graphene. According to the above results, the 3N-Co could serve as good SAC for the HER activity, while the OER overpotential over 4N-Co is only 0.38 eV. For comparison, previous results on HER and OER catalytic performance for the metal centered graphene and nitrogen-coordinated graphene were listed in Table S6. Therefore, N and Co co-doped graphene is a promising candidate as the bifunctional catalyst for electrocatalytic water splitting.

4. Conclusions

In summary, by using DFT calculations, we systematically investigated the activity sites for both HER and OER on late single transition-metal atom decorated N-doped graphene catalysts. It is found that the catalytic activity of SAC is highly correlated with the local environment of the active center as well as the d band energy level of TM. Both HER and OER performance can be well described by the negative

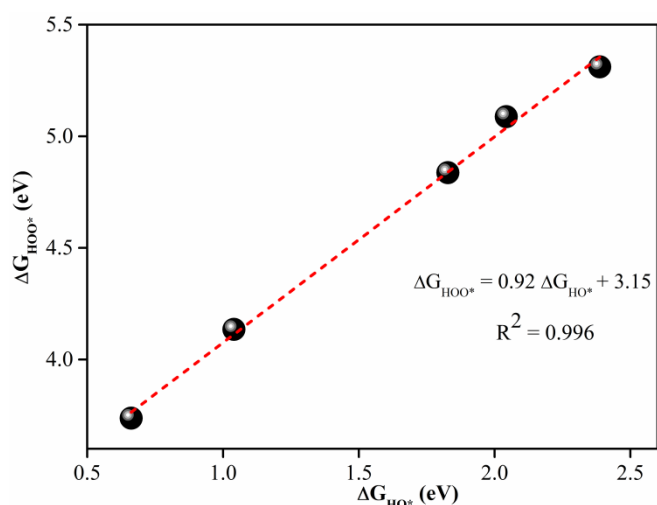


Fig. 6 The scaling relationship between ΔG_{HO^*} and ΔG_{HOO^*} for the systems we studied.

correlation between ΔG of adsorbents and ϵ_d of TMs for xN-TM catalysts. Among all the studied coordination number of xN-TM ($x=1\sim 4$), TM atomic sites with a lower coordinated number (3N-Co) exhibits the better HER performance, and the higher coordinated number of TM sites (4N-Co) presents the better OER performance, demonstrating the promise of Co and N co-doped graphene as the bifunctional catalyst for HER and OER. Our results provide a useful guidance in tuning HER and OER activity on the transition metal and N co-doped graphene as high-performance bifunctional electrocatalysts.

Conflicts of interest

There are no conflicts to declare.

Acknowledgements

This work was supported by the Assistant Secretary for Energy Efficiency and Renewal Energy of the U.S. Department of Energy under the Hydrogen Generation program. This theoretical work used the resources of the National Energy Research Scientific Computing Center (NERSC) that is supported by the Office of Science of the U. S. Department of Energy. We are grateful to the Chinese Scholarship Council (CSC) for providing the Ph.D. scholarship (Yanan Zhou) and to Lawrence Berkeley National Laboratory (United States) for financial support.

Notes and references

- Z. G. Yang, J. L. Zhang, M. C. W. Kintner-Meyer, X. C. Lu, D. Choi, J. P. Lemmon and J. Liu, *Chem. Rev.*, 2011, **111**, 3577-3613.
- N. L. Panwar, S. C. Kaushik and S. Kothari, *Renew. Sust. Energ. Rev.*, 2011, **15**, 1513-1524.
- G. S. Liu, S. J. You, Y. Tan and N. Q. Ren, *Environ. Sci. Technol.*, 2017, **51**, 2339-2346.
- H. B. Gray, *Nat. Chem.*, 2009, **1**, 7.
- Y. N. Zhou, W. Chu, F. L. Jing, J. Zheng, W. J. Sun and Y. Xue, *Appl. Surf. Sci.*, 2017, **410**, 166-176.
- F. Jiao and H. Frei, *Angew. Chem. Int. Edit.*, 2009, **48**, 1841-1844.
- D. M. Robinson, Y. B. Go, M. Mui, G. Gardner, Z. J. Zhang, D. Mastrogiovanni, E. Garfunkel, J. Li, M. Greenblatt and G. C. Dismukes, *J. Am. Chem. Soc.*, 2013, **135**, 3494-3501.
- S. Bai, C. M. Wang, M. S. Deng, M. Gong, Y. Bai, J. Jiang and Y. J. Xiong, *Angew. Chem. Int. Edit.*, 2014, **53**, 12120-12124.
- Y. Shiraishi, Y. Kofuji, S. Kanazawa, H. Sakamoto, S. Ichikawa, S. Tanaka and T. Hirai, *Chem. Commun.*, 2014, **50**, 15255-15258.
- X. Y. Lu and C. Zhao, *Nat. Commun.*, 2015, **6**, 6616..
- W. J. Zhou, X. J. Wu, X. H. Cao, X. Huang, C. L. Tan, J. Tian, H. Liu, J. Y. Wang and H. Zhang, *Energy Environ. Sci.*, 2013, **6**, 2921.
- H. Y. Jin, J. Wang, D. F. Su, Z. Z. Wei, Z. F. Pang and Y. Wang, *J. Am. Chem. Soc.*, 2015, **137**, 2688-2694.
- M. Gong, W. Zhou, M. C. Tsai, J. G. Zhou, M. Y. Guan, M. C. Lin, B. Zhang, Y. F. Hu, D. Y. Wang, J. Yang, S. J. Pennycook, B. J. Hwang and H. J. Dai, *Nat. Commun.*, 2014, **5**, 4695.
- L. L. Zhang, J. Xiao, H. Y. Wang and M. H. Shao, *ACS Catal.*, 2017, **7**, 7855-7865.
- H. Vrubel and X. L. Hu, *Angew. Chem. Int. Edit.*, 2012, **51**, 12703-12706.
- B. F. Cao, G. M. Veith, J. C. Neuefeind, R. R. Adzic and P. G. Khalifah, *J. Am. Chem. Soc.*, 2013, **135**, 19186-19192.
- H. T. Wang, Z. Y. Lu, S. C. Xu, D. S. Kong, J. J. Cha, G. Y. Zheng, P. C. Hsu, K. Yan, D. Bradshaw, F. B. Prinz and Y. Cui, *P. Natl. Acad. Sci. USA.*, 2013, **110**, 19701-19706.
- D. Merki and X. L. Hu, *Energy Environ. Sci.*, 2011, **4**, 3878.
- S. F. Fu, C. Z. Zhu, J. H. Song, M. H. Engelhard, X. L. Li, D. Du and Y. H. Lin, *ACS Energy Lett.*, 2016, **1**, 792-796.
- C. C. Lv, Q. P. Yang, Q. L. Huang, Z. P. Huang, H. Xia and C. Zhang, *J. Mater. Chem. A.*, 2016, **4**, 13336-13343.
- J. Q. Tian, Q. Liu, A. M. Asiri and X. P. Sun, *J. Am. Chem. Soc.*, 2014, **136**, 7587-7590.
- C. Z. Zhu, S. F. Fu, Q. R. Shi, D. Du, and Y. H. Lin, *Angew. Chem. Int. Edit.*, 2017, **56**, 13944-13960.
- X. F. Yang, A. Q. Wang, B. T. Qiao, J. Li, J. Y. Liu and T. Zhang, *Accounts. Chem. Res.*, 2013, **46**, 1740-1748.
- H. T. Wang, H. W. Lee, Y. Deng, Z. Y. Lu, P. C. Hsu, Y. Y. Liu, D. C. Lin and Y. Cui, *Nat. Commun.*, 2015, **6**, 7261.
- E. A. Hernández-Pagán, N. M. Vargas-Barbosa, T. H. Wang, Y. X. Zhao, E. S. Smotkin and T. E. Mallouk, *Energy Environ. Sci.*, 2012, **5**, 7582.
- G. P. Gao, S. Bottle and A. J. Du, *Catal. Sci. Technol.*, 2018, **8**, 996-1001.
- Y. Liang, Y. G. Li, H. L. Wang and H. J. Dai, *J. Am. Chem. Soc.*, 2013, **135**, 2013-2036.
- Q. Liu, J. Q. Tian, W. Cui, P. Jiang, N. Y. Cheng, A. M. Asiri and X. P. Sun, *Angew. Chem. Int. Edit.*, 2014, **53**, 6710-6714.
- D. P. He, Y. L. Xiong, J. L. Yang, X. Chen, Z. X. Deng, M. Pan, Y. D. Li and S. C. Mu, *J. Mater. Chem. A.*, 2017, **5**, 1930-1934.
- Y. Lin, Y. Pan, J. Zhang, Y. J. Chen, K. Sun, Y. Q. Liu and C. G. Liu, *Electrochim. Acta.*, 2016, **222**, 246-256.
- S. W. Liu, H. M. Zhang, Q. Zhao, X. Zhang, R. R. Liu, X. Ge, G. Z. Wang, H. J. Zhao and W. P. Cai, *Carbon*, 2016, **106**, 74-83.

- 32 B. R. Sathe, X. X. Zou and T. Asefa, *Catal. Sci. Technol.*, 2014, **4**, 2023-2030.
- 33 L. L. Zhang, W. Liu, Y. B. Dou, Z. Du and M. H. Shao, *J. Phys. Chem. C.*, 2016, **120**, 29047-29053.
- 34 X. C. Qiao, S. J. Liao, R. P. Zheng, Y. J. Deng, H. Y. Song and L. Du, *ACS Sustainable Chem. Eng.*, 2016, **4**, 4131-4136.
- 35 Z. L. Wang, X. F. Hao, Z. Jiang, X. P. Sun, D. Xu, J. Wang, H. X. Zhong, F. L. Meng and X. B. Zhang, *J. Am. Chem. Soc.*, 2015, **137**, 15070-15073.
- 36 G. Wu, A. Santandreu, W. Kellogg, S. Gupta, O. Ogoke, H. G. Zhang, H. L. Wang and L. M. Dai, *Nano Energy.*, 2016, **29**, 83-110.
- 37 A. Morozan, V. Goellner, Y. Nedellec, J. Hannauer and F. Jaouen, *J. Electrochem. Soc.*, 2015, **162**, H719-H726.
- 38 H. L. Fei, J. C. Dong, M. J. Arellano-Jimenez, G. L. Ye, N. Dong Kim, E. L. G. Samuel, Z. W. Peng, Z. Zhu, F. Qin, J. M. Bao, M. J. Yacaman, P. M. Ajayan, D. L. Chen and J. M. Tour, *Nat. Commun.*, 2015, **6**, 8668.
- 39 L. L. Fan, P. F. Liu, X. C. Yan, L. Gu, Z. Z. Yang, H. G. Yang, S. L. Qiu and X. D. Yao, *Nat. Commun.*, 2016, **7**, 10667.
- 40 H. X. Xu, D. J. Cheng, D. P. Cao and X. C. Zeng, *Nat. Catal.*, 2018, **1**, 339-348.
- 41 J. Q. Guan, Z. Y. Duan, F. X. Zhang, S. D. Kelly, R. Si, M. Dupuis, Q. G. Huang, J. Q. J. Chen, C. H. Tang and C. Li, *Nat. Catal.*, 2018, DOI: 10.1038/s41929-018-0158-6.
- 42 P. Z. Chen, T. P. Zhou, L. L. Xing, K. Xu, Y. Tong, H. Xie, L. D. Zhang, W. S. Yan, W. S. Chu, C. Z. Wu and Y. Xie, *Angew. Chem. Int. Edit.*, 2017, **56**, 610-614.
- 43 X. B. Liu, I. S. Amiinu, S. J. Liu, K. Cheng and S. C. Mu, *Nanoscale*, 2016, **8**, 13311-13320.
- 44 G. Kresse and J. Furthmuller, *Comp. Mater. Sci.*, 1996, **6**, 15-50.
- 45 G. Kresse and J. Furthmuller, *Phys. Rev. B.*, 1996, **54**.
- 46 P. E. Blöchl, *Phys. Rev. B.*, 1994, **50**, 17953-17979.
- 47 J. P. Perdew, K. Burke and M. Ernzerhof, *Phys. Rev. Lett.*, 1996, **77**.
- 48 J. P. Perdew, M. Ernzerhof and K. Burke, *J. Chem. Phys.*, 1996, **105**, 9982-9985.
- 49 S. Grimme, *J. Comput. Chem.*, 2006, **27**, 1787-1799.
- 50 L. Yu, X. L. Pan, X. M. Cao, P. Hu and X. H. Bao, *J. Catal.*, 2011, **282**, 183-190.
- 51 Y. Sha, T. H. Liu, B. V. Merinov and W. A. Goddard III, *J. Phys. Chem. Lett.*, 2010, **1**, 856-861.
- 52 K. Mathew, R. Sundararaman, K. Letchworth-Weaver, T. A. Arias and R. G. Hennig, *J. Chem. Phys.*, 2014, **140**, 084106.
- 53 R. K. Mathew and R. G. Henning, *arXiv preprint arXiv:1601.03346*, 2016.
- 54 J. K. Nørskov, T. Bligaard, A. Logadottir, J. R. Kitchin, J. G. Chen, S. Pandelov and U. Stimming, *J. Electrochem. Soc.*, 2005, **152**, J23.
- 55 B. Hinnemann, P. G. Moses, J. Bonde, K. P. Jørgensen, J. H. Nielsen, S. Horch, Ib. Chorkendorff and J. K. Nørskov, *J. Am. Chem. Soc.*, 2005, **127**, 5308-5309.
- 56 C. Tsai, F. Abild-Pedersen and J. K. Nørskov, *Nano Lett.*, 2014, **14**, 1381-1387.
- 57 J. K. Nørskov, J. Rossmeisl, A. Logadottir and L. Lindqvist, *J. Phys. Chem. B.*, 2004, **108**, 17886-17892.
- 58 M. T. Li, L. P. Zhang, Q. Xu, J. B. Niu and Z. H. Xia, *J. Catal.*, 2014, **314**, 66-72.
- 59 G. P. Gao, E. R. Waclawik and A. J. Du, *J. Catal.*, 2017, **352**, 579-585.
- 60 A. Valde, Z. W. Qu and G. J. Kroes, *J. Phys. Chem. C.*, 2008, **112**, 9872-9879.
- 61 P. Atkins and J. d. Paula, *Oxford University Press*, 2014.
- 62 D. Usachov, O. Vilkov, A. Gruneis, D. Haberer, A. Fedorov, V. K. Adamchuk, A. B. Preobrajenski, P. Dudin, A. Barinov, M. Oehzelt, C. Laubschat and D. V. Vyalikh, *Nano Lett.*, 2011, **11**, 5401-5407.
- 63 Q. Chen, A. W. Robertson, K. He, C. C. Gong, E. Yoon, A. I. Kirkland, G. D. Lee and J. H. Warner, *ACS Nano.*, 2016, **10**, 142-149.
- 64 W. Orellana, *J. Phys. Chem. C.*, 2013, **117**, 9812-9818.
- 65 P. Reunchan and S. H. Jhi, *Appl. Phys. Lett.*, 2011, **98**, 093103.
- 66 Y. X. Ouyang, C. Y. Ling, Q. Chen, Z. L. Wang, L. Shi and J. L. Wang, *Chem. Mater.*, 2016, **28**, 4390-4396.
- 67 V. Stamenkovic, B. S. Mun, K. J. J. Mayrhofer, P. N. Ross, N. M. Markovic, J. Rossmeisl, J. Greeley and J. K. Nørskov, *Angew. Chem. Int. Edit.*, 2006, **118**, 2963-2967.
- 68 M. Mavrikakis, B. Hammer and J. K. Nørskov, *Phys. Rev. Lett.*, 1998, **81**, 2819-2822.
- 69 C. Y. Ling, L. Shi, Y. X. Ouyang, X. C. Zeng and J. L. Wang, *Nano Letter.*, 2017, **17**, 5133-5139.
- 70 M. P. Browne, H. Nolan, G. S. Duesberg, P. E. Colavita and M. E. G. Lyons, *ACS Catal.*, 2016, **6**, 2408-2415.
- 71 D. Friebel, M. W. Louie, M. Bajdich, K. E. Sanwald, Y. Cai, A. M. Wise, M. J. Cheng, D. Sokaras, T. C. Weng, R. Alonso-Mori, R. C. Davis, J. R. Bargar, J. K. Nørskov, A. Nilsson and A. T. Bell, *J. Am. Chem. Soc.*, 2015, **137**, 1305-1313.
- 72 I. C. Man, H. Y. Su, F. Calle-Vallejo, H. A. Hansen, J. I. Martínez, N. G. Inoglu, J. Kitchin, T. F. Jaramillo, J. K. Nørskov and J. Rossmeisl, *ChemCatChem*, 2011, **3**, 1159-1165.
- 73 S. Zhou, N. S. Liu, Z. Y. Wang and J. J. Zhao, *ACS Appl. Mater. Interfaces.*, 2017, **9**, 22578-22587.
- 74 X. L. Zhang, Z. X. Yang, Z. S. Lu and W. C. Wang, *Carbon*, 2018, **130**, 112-119.

Graphical abstract

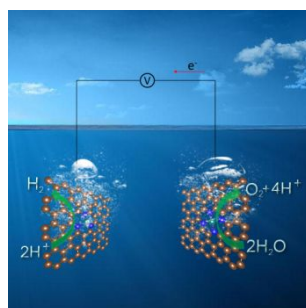
Transition-metal single atoms in nitrogen-doped graphene as efficient active centers for water splitting: A theoretical study

Yanan Zhou,^{‡^{ab}} Guoping Gao,^{‡^b} Yan Li,^c Wei Chu,^{*^a} and Lin-Wang Wang^{*^b}

^a School of Chemical Engineering, Sichuan University, Chengdu, 610065, Sichuan, China

^b Materials Science Division, Lawrence Berkeley National Laboratory, Berkeley, 94720, California, United States

^c State Key Laboratory for Mechanical Behavior of Materials, Xi'an Jiaotong University, Xi'an, 710049, Shaanxi, China



The triple-coordinated Co exhibits high catalytic activity toward HER with the calculated hydrogen adsorption free energy of -0.01 eV, and quadruple-coordinated Co shows excellent catalytic performance for OER with a low computed overpotential of -0.39 V.